Opto-Electronic Advances

ISSN 2096-4579 CN 51-1781/TN

Broadband all-fiber optical phase modulator based on photo-thermal effect in a gas-filled hollow-core fiber

Shoulin Jiang, Feifan Chen, Yan Zhao, Shoufei Gao, Yingying Wang, Hoi Lut Ho and Wei Jin

Citation: Jiang SL, Chen FF, Zhao Y, Gao SF, Wang YY et al. Broadband all-fiber optical phase modulator based on photo-thermal effect in a gas-filled hollow-core fiber. *Opto-Electron Adv* **6**, 220085(2023).

https://doi.org/10.29026/oea.2023.220085

Received: 7 May 2022; Accepted: 8 August 2022; Published online: 4 November 2022

Opto-Electronic Advances

Article

May 2023, Vol. 6, No. 5

DOI: 10.29026/oea.2023.220085

Broadband all-fiber optical phase modulator based on photo-thermal effect in a gas-filled hollow-core fiber

Shoulin Jiang[1], Feifan Chen[1,2], Yan Zhao[1,2], Shoufei Gao[3], Yingying Wang[3], Hoi Lut Ho[1,2] and Wei Jin[1,2]*

We report broadband all-fiber optical phase modulation based on the photo-thermal effect in a gas-filled hollow-core fiber. The phase modulation dynamics are studied by multi-physics simulation. A phase modulator is fabricated using a 5.6-cm-long anti-resonant hollow-core fiber with pure acetylene filling. It has a half-wave optical power of 289 mW at 100 kHz and an average insertion loss 0.6 dB over a broad wavelength range from 1450 to 1650 nm. The rise and fall time constants are 3.5 and 3.7 μs, respectively, 2–3 orders of magnitude better than the previously reported microfiber-based photo-thermal phase modulators. The gas-filled hollow-core waveguide configuration is promising for optical phase modulation from ultraviolet to mid-infrared which is challenging to achieve with solid optical fibers.

Keywords: optical modulators; photo-thermal effects; hollow-core fibers

Jiang SL, Chen FF, Zhao Y, Gao SF, Wang YY et al. Broadband all-fiber optical phase modulator based on photo-thermal effect in a gas-filled hollow-core fiber. *Opto-Electron Adv* **6**, 220085 (2023).

Introduction

Phase modulators are key components in optical communication, sensing, and signal processing systems. All-optical modulators, which modulate the phase or intensity of a light signal by a control light beam, have attracted great research attentions[1–13]. Based on stimulated Brillouin scattering and cross-phase modulation, all-optical phase shifters with fast response have been demonstrated[3,4]. However, due to the intrinsic weak nonlinearity of silica, high-power control beams and long optical fibers are required to make useful devices. Yu et al. reported an all-optical phase modulator using a graphene-coated microfiber (MF)[5]. Utilizing the evanescent field of the MF and the strong Kerr nonlinearity of graphene, phase modulation up to 0.18π rad was achieved with a graphene coated length of 15 μm. However, it is challenging to further enhance the phase modulation by reducing the fiber diameter or coating a longer length of fiber with graphene, which will lead to significantly increased insertion loss (IL) due to the intrinsic absorption and imperfect coating of graphene.

All-optical phase modulators have also been demonstrated based on the photo-thermal (PT) effect in nano-waveguides and microfibers coated with low-dimensional materials[6–13]. Nano-waveguide-based phase modulators are compact in size and have fast response, but the

[1]Photonics Research Center, the Hong Kong Polytechnic University Shenzhen Research Institute, Shenzhen 518057, China; [2]Department of Electrical Engineering and Photonics Research Institute, the Hong Kong Polytechnic University, Hong Kong 999077, China; [3]Institute of Photonics Technology, Jinan University, Guangzhou 510632, China.

*Correspondence: Jin W, E-mail: wei.jin@polyu.edu.hk

Received: 7 May 2022; Accepted: 8 August 2022; Published online: 4 November 2022

coupling loss is large when connecting with optical fibers[6,7]. Gan et al. demonstrated a MF-based PT optical phase modulator with graphene coating[8]. Graphene absorption of the evanescent field of a control light beam heats up the MF, and modulates the refractive index of silica. With a control light power of 230 mW, a signal phase change of 21π is achieved. The IL of the device is 5.4 dB at 1540 nm, mainly due to the absorption of graphene. MF-based PT phase modulators have also been demonstrated with other low-dimensional materials, including tungsten disulfide (WS_2)[9], phosphorene[10], bismuthene[11], boron nanosheets[12], and boron quantum dots (BQDs)[13]. These phase modulators typically have high IL, limited by the absorption and imperfect deposition of low-dimensional materials, and long response time of several milliseconds.

In this work, we demonstrate a new type of all-fiber optical phase modulator based on a gas-filled hollow-core fiber (HCF). In the HCF, most of the optical mode power propagates in the hollow core, which is free from absorption of the solid fiber materials. This enables extremely broadband low-loss transmission, from the ultraviolet to the mid-infrared, apart from a few narrow resonant loss bands[14–18]. The HCF can confine gas phase material, a high intensity control beam and a signal beam simultaneously in the hollow core, providing an ideal platform for strong light-gas interaction over a long interaction length[19,20]. The broad transmission band of the HCF in combination with narrow absorption lines of the gas material enables broadband modulators which are challenging to realize with solid core fibers.

Principle and multi-physics simulation

Figure 1(a) shows the basic idea of the HCF-based optical phase modulator. Optical absorption of the control beam excites gas molecules to a higher energy level, which releases heat through non-radiative relaxation. This changes the gas temperature (T) and pressure (p) in the hollow core, which modulates the effective refractive index and hence the phase of the signal beam propagating through the HCF. By modulating the intensity of the control beam, the phase of signal beam is modulated accordingly.

Acetylene (C_2H_2) is selected as the filling gas because it has strong absorption lines at the edge of C-band, which enables a compact modulator with a cost-effective

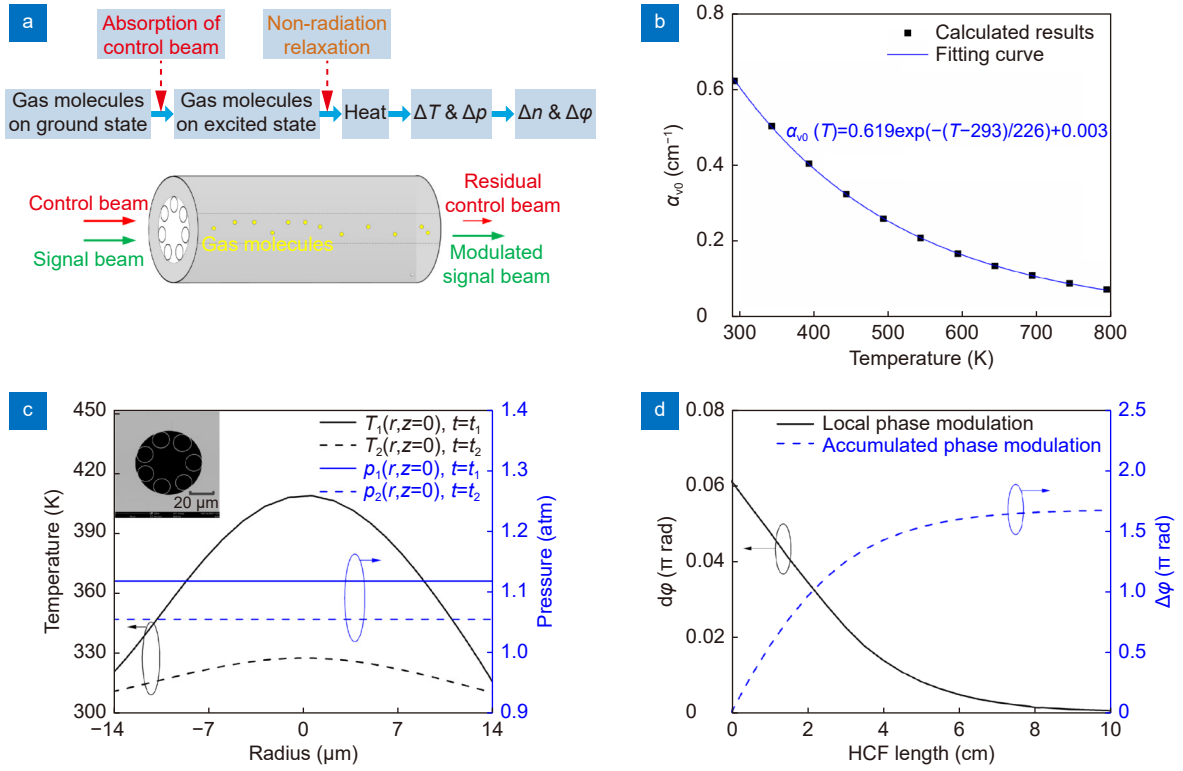

Fig. 1 | (**a**) Schematic showing the principle of HCF-based PT phase modulator. (**b**) Calculated absorption coefficient of the P(9) line of pure C_2H_2 at 1 atm as a function of T by use of HITRAN database[22]. (**c**) Transverse distribution of T and p calculated by using COMSOL Multiphysics with P_{ctrl}=500 mW and f=100 kHz. (**d**) Variation of local phase modulation with a step length of 1 mm and accumulated phase modulation along the length of an acetylene-filled HCF.

control light source. Besides, C_2H_2 is nontoxic and has ro-vibrational relaxation time of 74 ns at P(9) absorption line[21], which is much faster than the heat conduction time from the gas core to the silica cladding with a typical value of several microseconds. The wavelength of the control beam is fixed at the center of the P(9) absorption line of C_2H_2 at 1530.371 nm. The absorption coefficient is almost independent of pressure around 1 atm according to HITRAN database[22] and can be fitted to an exponential function of temperature as shown in Fig. 1(b).

The HCF considered here is an anti-resonant hollow-core fiber (AR-HCF) with a mode field diameter of 22 μm at 1550 nm and its SEM image is shown in the inset of Fig. 1(c). The AR-HCF has a broad transmission window with transmission loss less than 3 dB/m from 1200 nm to 2200 nm. When the control light power is sinusoidally modulated, the heat source $Q(r,z,t)$ due to PT effect may be expressed as:

$$Q(r,z,t) = \alpha_{v0}(r,z)P_{\mathrm{ctrl}}(z)\psi_{\mathrm{nor,ctrl}}(r)[\sin(2\pi ft)+1]\ , \quad (1)$$

where $P_{\mathrm{ctrl}}(z)$, $\psi_{\mathrm{nor,ctrl}}(r)$ and f represent the average power, normalized intensity distribution and modulation frequency of control beam, respectively. It should be noted that the absorption coefficient α_{v0} is related to both the radial position r and the axial position z. This is because that α_{v0} depends on temperature, which is non-uniform in the cross-section and along the HCF.

Based on the fiber structure shown in Fig. 1(c), we have simulated the distribution of temperature and pressure inside the HCF based on the compressible flow equations using COMSOL Multiphysics software[23,24]. The main thermodynamic parameters of materials used for simulation are shown in Table 1[25,26]. The calculated results for P_{ctrl}=500 mW and f=100 kHz are shown in Fig. 1(c). Here the moments when the temperature reaches maximum and minimum are labeled as t_1 and t_2, respectively. Within a modulation period, T changes up to 80 K in the core center and p changes only about 0.06 atm which is independent of the radial position.

The phase modulation of signal beam at position z within a step length dz may be calculated by using[27]:

$$\begin{aligned}\mathrm{d}\varphi(z) &= \frac{2\pi \mathrm{d}z}{\lambda}\iint \Delta n(r,z)\psi_{\mathrm{nor,sig}}(r)\mathrm{d}A \\ &= \frac{2\pi \mathrm{d}z}{\lambda}\iint \left[\frac{\mu p_2(z)}{T_2(r,z)} - \frac{\mu p_1(z)}{T_1(r,z)}\right]\psi_{\mathrm{nor,sig}}(r)\mathrm{d}A \\ &= \frac{2\pi \mathrm{d}z}{\lambda} \\ &\quad \cdot \iint \left[-\frac{\mu p_2(z)}{T_1(r,z)T_2(r,z)}\Delta T(r,z) + \frac{\mu}{T_1(r,z)}\Delta p(z)\right] \\ &\quad \psi_{\mathrm{nor,sig}}(r)\mathrm{d}A\ , \end{aligned} \quad (2)$$

where λ and $\psi_{\mathrm{nor,sig}}(r)$ represent the wavelength and normalized intensity distribution of signal beam, respectively, and μ equals to 0.154 K/atm for pure C_2H_2. According to Eq. (2), d$\varphi(z)$ along the HCF with a step length of 1 mm is calculated as the solid black line shows in Fig. 1(d). Due to gas absorption, the control light power $P_{\mathrm{ctrl}}(z)$ reduces with propagation distance, resulting in a decrease of the phase modulation along the fiber length. As a result, the accumulated phase modulation increases nonlinearly with the fiber length, which increases only slightly from 1.53π rad to 1.67π rad when the HCF length doubles from 5 cm to 10 cm.

Fabrication and characterization connector

The schematic of the fabricated gas-filled HCF phase modulator module is shown in Fig. 2(a). Thermally expanded core fibers (TECFs), directly fabricated by heating standard single mode fiber (SSMF) locally to expand its mode field diameter to 22 μm, with anti-reflective coating (R<0.25% at 1550 nm) were used to reduce the connection loss[17,18]. Both ends of a 5.6-cm-long AR-HCF were packaged using capillary glass tubes with inner and outer diameter of 230 μm and 1.8 mm, respectively. It is then inserted into a 5-cm-long hollow glass tube with inner diameter of 1.81 mm and fixed with glue. The HCF and two TECFs were precisely aligned using a pair of 5-axis alignment stages and fixed using a 5-mm-long glass connectors with inner diameter of 1.81 mm. There is a micro hole on the glass connector which allows gas diffusion freely. After the low-loss connection between

Table 1 | Temperature-dependent thermodynamic parameters of materials at 1 atm[25,26].

Material	Acetylene		Silica		Air	
Temperature T [K]	300	400	300	400	300	400
Density ρ [kg/m^3]	1.04	0.78	2203	2203	1.16	0.85
Thermal conductivity κ [W/(m·K)]	0.0214	0.0333	1.38	1.48	0.0262	0.0333
Heat capacity C_p [J/(kg·K)]	1699	1938	746	891	1007	1018

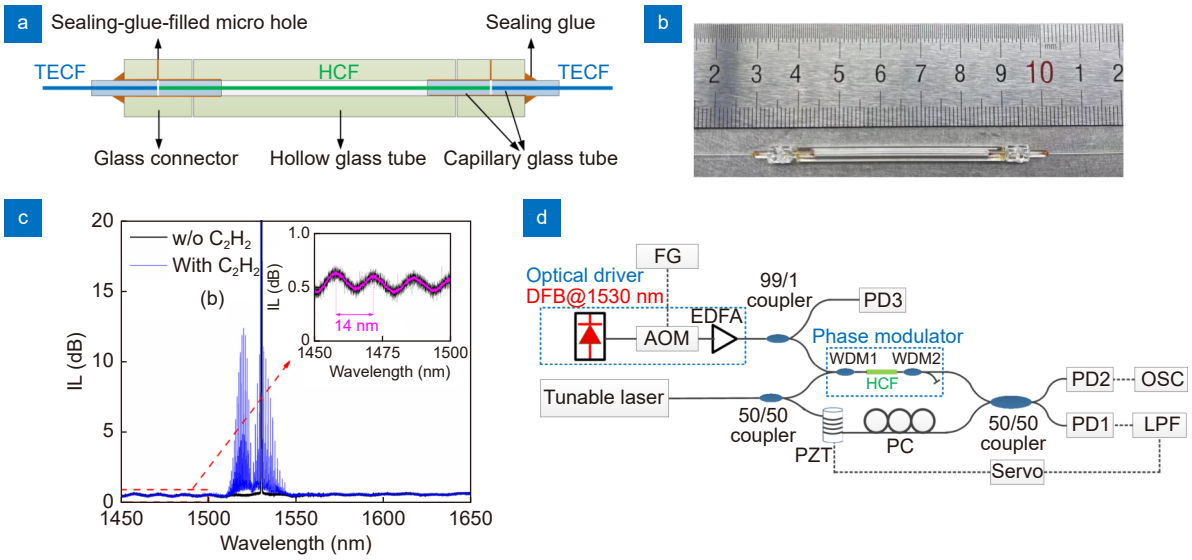

Fig. 2 | (**a**) Schematic diagram and (**b**) photo of the fabricated gas-filled hollow-core fiber phase modulator. (**c**) Measured loss spectrum of the phase modulator. (**d**) Experimental setup for characterizing the phase modulator. TECF: thermal-expanded core fiber, DFB: distributed feedback laser, FG: function generator, AOM: acoustic optical modulator, EDFA: erbium-doped fiber amplifier, WDM: wavelength-division multiplexer, PZT: piezoelectric transducer, PC: polarization controller, PD: photodetector, OSC: oscilloscope, LPF: low-pass filter.

different fibers, we put the module in a glove box with inner volume of 1 L and pure C_2H_2 was filled into the box with a flow rate of 300 sccm to replace the air. The loss spectrum of the module was monitored using a supercontinuum source and an optical spectrum analyzer. As the gas filling, the absorption loss at 1530.371 nm gradually increased and reached its maximum after about 15 min. The C_2H_2 concentration inside the HCF was close to be 100% with gas pressure of 1 atm. The micro holes were sealed with glue in the box and a compact gas-filled HCF module was fabricated as shown in Fig. 2(b). The module forms the PT phase modulator together with two wavelength-division multiplexers (WDMs). WDM1 was used to combine the control beam and the signal beam. WDM2 based on thin-film filter reflected the unabsorbed control beam within 1530.3±0.4 nm and passed the signal beam at other wavelength. It can also be replaced by other optical filters such as a fiber Bragg grating.

Figure 2(c) shows the loss spectrums of the device before and after C_2H_2 filling. The average IL without C_2H_2 filling is about 0.6 dB with a wavelength-dependent loss about 0.2 dB from 1450 to 1650 nm, except for the higher loss induced by the WDMs at 1530.3±0.4 nm. The wavelength dependent loss shows a beat period of 14 nm, which coincides well with the calculated mode effective index difference of 3.0×10^{-3} between LP_{01} and LP_{02} mode in the AR-HCF and the mode extinction ratio of LP_{02} mode is estimated to be 40 dB. It can be further suppressed by optimizing mode field matching or using HCF with better mode purity. The beating corresponding to the interference of LP_{01} and LP_{11} mode is not observable, thanks to the accurate alignments. After C_2H_2 filling, the overall loss keeps unchanged while additional loss peaks appear due to C_2H_2 absorption, which are shown as the blue lines.

The phase modulator was characterized by using the setup shown in Fig. 2(d). Light beam from a distributed feedback (DFB) laser at 1530.371 nm was modulated by an acoustic optical modulator (AOM) and amplified by an erbium-doped fiber amplifier (EDFA), which acts as the control beam with intensity modulation. A wavelength tunable laser covering wavelength from 1480 to 1640 nm was used as the signal light source. The phase modulator under test formed the one arm of the Mach-Zehnder interferometer (MZI) and a segment of SMF coiled on a piezoelectric transducer (PZT) worked as the second arm. The voltage applied on the PZT was feedback controlled by using the output from PD1 to keep MZI at quadrature. PD2 and PD3 were used to detect the phase modulation and monitor the power level of the control beam, respectively.

Results and discussion

The control light power was sinusoidally modulated at 100 kHz and the P_{ctrl} in the HCF was estimated considering the connection loss between SMF and HCF. Figure 3(a) shows the MZI output waveforms at 1550 nm with

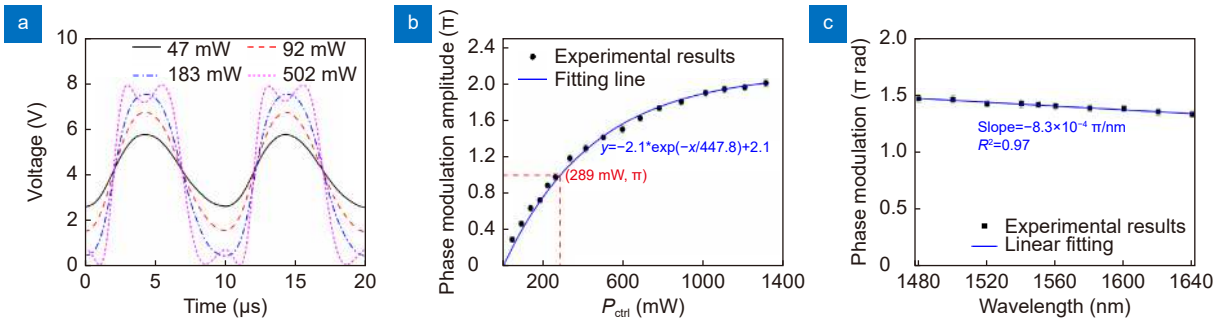

Fig. 3 | Characteristics of the HCF-based PT phase modulator with a modulation frequency of 100 kHz. (**a**) MZI output waveforms with different P_{ctrl} in the AR-HCF. (**b**) Phase modulation amplitude as a function of P_{ctrl}. (**c**) Wavelength dependence of phase modulation amplitude for P_{ctrl}=502 mW.

different P_{ctrl}. The amplitude of the signal phase modulation is determined from the time-domain MZI output waveform[28], which increases nonlinearly with P_{ctrl} as shown in Fig. 3(b). Here we define the control light power required to achieve the phase modulation amplitude of π rad as the half-wave power P_{π}, which is determined by curve fitting to be 289 mW at 100 kHz. We believe that the temperature change at high P_{ctrl} is responsible for the nonlinear response. As P_{ctrl} increases, the gas temperature in the HCF also increases, leading to reduced absorption coefficient and gas density, as well as increased heat capacity and heat conductivity of C_2H_2 at the core center. These different factors contribute to the nonlinear response observed in Fig. 3(b). Due to the above reasons, the phase modulation decreases from 1.41π rad to 1.23π rad at 1550 nm when the environment temperature rises from 25 °C to 100 °C. The temperature-dependence of the phase modulator may be minimized by optimizing gas concentration and fiber length.

We also investigated the wavelength dependence of the PT phase modulation and the result is shown in Fig. 3(c). According to Eq. (2), the phase modulation has a $1/\lambda$ dependence, and it is approximately linear with λ over a small wavelength span from 1480 nm to 1640 nm with an average decline rate of -8.3×10^{-4} π rad/nm.

The frequency response at 1550 nm with P_{ctrl} =502 mW is shown in Fig. 4(a). As the frequency increases from 10 kHz to 1 MHz, the phase modulation decreases from 1.92π to 0.22π with a 3-dB modulation bandwidth of 180 kHz.

The response time is investigated using square pulses with frequency of 10 kHz and duty cycle of 50%, shown as the black dotted line in Fig. 4(b). The MZI output received by PD2 shows a near-square waveform which confirms the fast response of the phase modulator. By fitting to exponential functions, the rise and fall time constants are determined to be 3.5 μs and 3.7 μs, respectively. For HCF-based PT phase modulators, the heat source locates at the gas core region and the heat dissipates quickly once it reaches the silica cladding, whose thermal conductivity is 53 times higher than that of the air. The characteristic time constant is mainly limited by the thermal conduction time from the gas core to the silica cladding with typical value of several microseconds. However, for MF-based PT phase modulators, the heat source surrounds the MF with diameter about several micrometers and the heat dissipates through the 2D-material/air interface. Due to the low thermal conductivity of surrounding air, longer time is required to reach thermal equilibrium. It benefits the heat accumulation and hence higher phase change, but comprises the response time to milliseconds level.

Table 2 summarizes the performances of state-of-the-art all-fiber optical phase modulators. The HCF-based PT phase modulator reported here shows impressive overall performance with moderate phase modulation ability and low IL over a broad wavelength band. Benefited from the high thermal conductivity of silica cladding, the response time of our modulator is 2-3 orders faster than the MF-based PT phase modulators working in the air[8–13]. Without fiber tapering and low-dimensional material deposition, the gas-filled HCF-based PT phase modulator is easy to fabricate. Compared with commercial electro-optics modulators, the HCF-based PT phase modulator has unique merits, including ultra-low loss within a wide wavelength span, all-optical and hence immune to electromagnetic interference, high power handing capability. It would have promising applications in fiber optic interferometer-based phase demodulation systems in particular for harsh environment and remote applications[2,29], as well as for all-fiber actively Q-switched lasers[13].

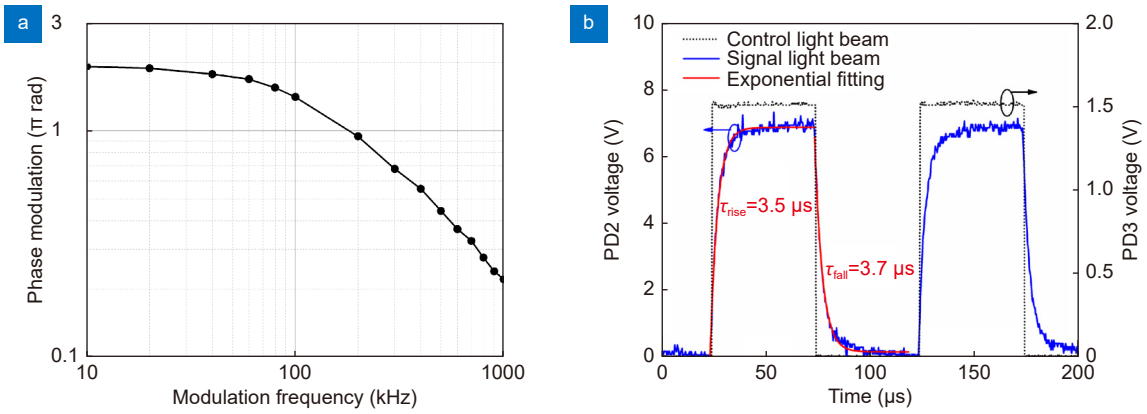

Fig. 4 | (**a**) Frequency response of phase modulation with P_{ctrl} =502 mW. (**b**) Transient response detected by use of the MZI for control light beam pulse width of 50 μs.

Table 2 | Summary of state-of-the-art all-fiber optical phase modulators.

Ref.	Physical effect	Fiber type	Functional material	Phase change (rad)	Rise/fall time constant	Insertion loss
ref.[5]	Kerr	MF	Graphene	0.18π@1.15 W[a]	a few ns	10 dB@1550 nm
ref.[8]	PT	MF	Graphene	21π@230 mW[a]	4.0/1.4 ms	5.4 dB@1540 nm
ref.[9]	PT	MF	Phosphorene	8π@290 mW[a]	2.5/2.1 ms	10 dB @1550 nm
ref.[10]	PT	MF	WS_2	6π@345 mW[a]	7.3/3.5 ms	3.5 dB@1550 nm
ref.[11]	PT	MF	Bismuthene	22π@420 mW[a]	3.4/3.4 ms	5.5 dB@1550 nm
ref.[12]	PT	MF	Boron nanosheet	4π@300 mW[a]	0.48/0.69 ms	5.5 dB@1550 nm
ref.[13]	PT	MF	BQDs	10π@315 mW[a]	0.5/0.6 ms	Not given
This work	PT	AR-HCF	C_2H_2	π@289 mW[b]	3.5/3.7 μs	0.6 dB@1550 nm

[a] peak phase modulation for a step change of control power, [b] dynamic phase modulation measured at 100 kHz.

Conclusions

In summary, we have reported, for the first time to our knowledge, an optically controlled all-fiber PT phase modulator based on a gas-filled HCF. Preliminary experiment achieves effective optical phase modulation with a half-wave power of 289 mW at 100 kHz. It shows impressive low IL of ~0.6 dB and broad operational wavelength band from 1480 to 1640 nm. The measured rise and fall time constants are 3.5 μs and 3.7 μs, respectively, 2–3 orders of magnitude faster than the reported MF-based PT phase modulators. The modulator performance could be further improved by optimizing the HCF structure and length as well as gas composition and pressure. The broad transmission bands of the state-of-the-art HCFs in combination with the many available gas species would allow the development of all-optical modulators from ultraviolet to mid-infrared, which are quite challenging to realize with solid state materials.

References

1. Sturm C, Tanese D, Nguyen HS, Flayac H, Galopin E et al. All-optical phase modulation in a cavity-polariton Mach–Zehnder interferometer. *Nat Commun* **5**, 3278 (2014).
2. Li MW, Yu Y, Lu Y, Hu XY, Wang YR et al. Optical microfiber all-optical phase modulator for fiber optic hydrophone. *Nanomaterials* **11**, 2215 (2021).
3. Loayssa A, Lahoz FJ. Broad-band RF photonic phase shifter based on stimulated Brillouin scattering and single-sideband modulation. *IEEE Photonics Technol Lett* **18**, 208–210 (2006).
4. Sharping JE, Fiorentino M, Kumar P, Windeler RS. All-optical switching based on cross-phase modulation in microstructure fiber. *IEEE Photonics Technol Lett* **14**, 77–79 (2002).
5. Yu SL, Wu XQ, Chen KR, Chen BG, Guo X et al. All-optical graphene modulator based on optical Kerr phase shift. *Optica* **3**, 541–544 (2016).
6. Qiu CY, Yang YX, Li C, Wang YF, Wu K et al. All-optical control of light on a graphene-on-silicon nitride chip using thermo-optic effect. *Sci Rep* **7**, 17046 (2017).
7. Cheng Z, Cao R, Guo J, Yao YH, Wei KK et al. Phosphorene-assisted silicon photonic modulator with fast response time. *Nanophotonics* **9**, 1973–1979 (2020).
8. Gan XT, Zhao CY, Wang YD, Mao D, Fang L et al. Graphene-assisted all-fiber phase shifter and switching. *Optica* **2**, 468–471 (2015).
9. Wu K, Wang YF, Qiu CY, Chen JP. Thermo-optic all-optical devices based on two-dimensional materials. *Photonics Res* **6**, C22–C28 (2018).
10. Wang YZ, Zhang F, Tang X, Chen X, Chen YX et al. All-optical phosphorene phase modulator with enhanced stability under ambient conditions. *Laser Photonics Rev* **12**, 1800016 (2018).
11. Wang YZ, Huang WC, Zhao JL, Huang H, Wang C et al. A

bismuthene-based multifunctional all-optical phase and intensity modulator enabled by photothermal effect. *J Mater Chem C* **7**, 871–878 (2019).
12. Guo QB, Wu K, Shao ZP, Basore ET, Jiang P et al. Boron nanosheets for efficient all-optical modulation and logic operation. *Adv Opt Mater* **7**, 1900322 (2019).
13. Wang C, Chen QY, Chen HL, Liu J, Song YF et al. Boron quantum dots all-optical modulator based on efficient photothermal effect. *Opto-Electron Adv* **4**, 200032 (2021).
14. Gao SF, Wang YY, Ding W, Hong YF, Wang P. Conquering the Rayleigh scattering limit of silica glass fiber at visible wavelengths with a hollow-core fiber approach. *Laser Photonics Rev* **14**, 1900241 (2020).
15. Cassataro M, Novoa D, Günendi MC, Edavalath NN, Frosz MH et al. Generation of broadband mid-IR and UV light in gas-filled single-ring hollow-core PCF. *Opt Express* **25**, 7637–7644 (2017).
16. Sakr H, Hong Y, Bradley TD, Jasion GT, Hayes JR et al. Interband short reach data transmission in ultrawide bandwidth hollow core fiber. *J Lightwave Technol* **38**, 159–165 (2020).
17. Zhang Z, Ding W, Jia AQ, Hong YF, Chen Y et al. Connector-style hollow-core fiber interconnections. *Opt Express* **30**, 15149–15157 (2022).
18. Suslov D, Komanec M, Fokoua ERN, Dousek D, Zhong AL et al. Low loss and high performance interconnection between standard single-mode fiber and antiresonant hollow-core fiber. *Sci Rep* **11**, 8799 (2021).
19. Jin W, Cao YC, Yang F, Ho HL. Ultra-sensitive all-fibre photothermal spectroscopy with large dynamic range. *Nat Commun* **6**, 6767 (2015).
20. Zhao Y, Qi Y, Ho HL, Gao SF, Wang YY et al. Photoacoustic Brillouin spectroscopy of gas-filled anti-resonant hollow-core optical fibers. *Optica* **8**, 532–538 (2021).
21. Wang JCF, Springer GS. Vibrational relaxation times in some hydrocarbons in the range 300–900°K. *J Chem Phys* **59**, 6556–6562 (1973).
22. Gordon IE, Rothman LS, Hill C, Kocharov RV, Tan Y et al. The HITRAN2016 molecular spectroscopic database. *J Quant Spectrosc Radiat Transfer* **203**, 3–69 (2017).
23. Bialkowski SE. *Photothermal Spectroscopy Methods for Chemical Analysis* (John Wiley & Sons, New York, 1996).
24. Batchelor GK. *An Introduction to Fluid Dynamics* (Cambridge University Press, New York, 2000).
25. Weber MJ. *Handbook of Optical Materials* (CRC Press, Boca Raton, 2018).
26. Lide DR. *CRC Handbook of Chemistry and Physics*: *A Ready-Reference Book of Chemical and Physical Data* (CRC Press, Boca Raton, 2004).
27. Owens JC. Optical refractive index of air: dependence on pressure, temperature and composition. *Appl Opt* **6**, 51–59 (1967).
28. Jin W, Uttamchandani D, Culshaw B. Direct readout of dynamic phase changes in a fiber-optic homodyne interferometer. *Appl Opt* **31**, 7253–7258 (1992).
29. Yang LY, Li YP, Fang F, Li LY, Yan ZJ et al. Highly sensitive and miniature microfiber-based ultrasound sensor for photoacoustic tomography. *Opto-Electron Adv* **5**, 200076 (2022).

Acknowledgements

We are grateful for financial supports from the National Key Research and Development Program of China (2019YFB2203904), the National Natural Science Foundation of China (U21A20506, 62105122, 61827820, 62005233), the Shenzhen STIC Funding (RCBS20200714114819032), the Local Innovative and Research Teams Project of Guangdong Pear River Talents Program (2019BT02X105).

Author contributions

W. Jin proposed the original idea and supervised the project. S. L. Jiang designed the research. Y. Zhao and S. L. Jiang built the model and performed the simulation. S. F. Gao and Y. Y. Wang fabricated the hollow-core fibers. S. L. Jiang, F. F. Chen and H. L. Ho fabricated the sample, performed the experiments and analysed the data. All authors discussed and commented on the manuscript.

Competing interests

The authors declare no competing financial interests.